Pacific Northwest
NATIONAL LABORATORY

PNNL-38958

Mesofluidic Inline Separation for Produced Water Treatment (CRADA 537)

October 2025

Carolyn A Burns
Sarah Suffield
Chinmayee Subban
Michael J Minette
Leonard F Pease

U.S. DEPARTMENT OF ENERGY

Prepared for the U.S. Department of Energy
under Contract DE-AC05-76RL01830

DISCLAIMER

PACIFIC NORTHWEST NATIONAL LABORATORY
operated by
BATTELLE
for the
UNITED STATES DEPARTMENT OF ENERGY
under Contract DE-AC05-76RL01830

Printed in the United States of America

Available to DOE and DOE contractors from the
Office of Scientific and Technical Information,
P.O. Box 62, Oak Ridge, TN 37831-0062;
ph: (865) 576-8401
fax: (865) 576-5728
email: reports@adonis.osti.gov

Available to the public from the National Technical Information Service
5301 Shawnee Rd., Alexandria, VA 22312
ph: (800) 553-NTIS (6847)
email: orders@ntis.gov <https://www.ntis.gov/about>
Online ordering: http://www.ntis.gov

PNNL-38958

Mesofluidic Inline Separation for Produced Water Treatment (CRADA 537)

October 2025

Carolyn A Burns
Sarah Suffield
Chinmayee Subban
Michael J Minette
Leonard F Pease

Prepared for
the U.S. Department of Energy
under Contract DE-AC05-76RL01830

Pacific Northwest National Laboratory
Richland, Washington 99354

Cooperative Research and Development Agreement (CRADA) Final Report

Report Date: October 2025

In accordance with Requirements set forth in the terms of the CRADA, this document is the CRADA Final Report, including a list of Subject Inventions, to be provided to PNNL Information Release who will forward to the DOE Office of Scientific and Technical Information as part of the commitment to the public to demonstrate results of federally funded research.

Parties to the Agreement: PNNL, APEX Petroleum Engineering

CRADA number: PNNL 537

CRADA Title: Mesofluidic Inline Separation for Produced Water Treatment

Responsible Technical Contact at DOE Lab: Leonard Pease

Name and Email Address of POC at Company: Monica Chavez <monica.chavez@pnnl.gov>

DOE Program Office: Fossil Energy and Carbon Management

Joint Work Statement Funding Table showing DOE funding commitment: The Government's estimated contribution, which is provided through PNNL's contract with DOE, is $246,960, subject to available funding (see Table 1).

Table 1. Joint Work Statement Funding Table (as planned)

	Year 1		Year 2		**Total**	
Funding Type	Funds-in	In-kind	Funds-in	In-kind	Funds-in	In-kind
Apex PE, LLC		$170,956		$76,202		$246,976
Dept. of Energy/PNNL	$171,650		$75,310		$246,960	
Totals	**$342,606**		**$151,512**		**$493,936**	

Executive Summary

Mesofluidic inline separation developed by PNNL represents an opportunity to remove a key barrier in the treatment of produced water, namely suspended solids that clog downstream operations. The US alone produces over 800 billion gallons of produced water each year, most of which is reinjected underground (but not into the aquifers) as waste. The impact from treating and reusing even a fraction of this wastewater is immense as aquifers in the Midwest and elsewhere dry. The work described herein is essential to leveraging the opportunity to improve produced water quality (to allow for beneficial use) by combining mesofluidic inline separators with reverse osmosis systems. Providing water for agricultural and industrial uses in the American Southwest and Midwest by allowing the reuse of petroleum produced water may be critical to the long-term economics of the region. This is especially true as drought conditions are rapidly lowering aquifer levels in these regions. The incumbent technology for desalination is reverse osmosis (RO) due to its ability to treat a wide range of feedwaters and technological maturity. However, suspended solids cause RO (and other dissolved solids removal technologies) to become clogged and lose performance. A common strategy is to use prefilters upstream of RO systems, but these membrane-based filters easily clog and require regular maintenance. Unlike membrane filters, mesofluidic inline separators provide removal of suspended solids with much lower pressure drops than conventional filtration systems, permitting substantially higher flowrates. Although the amount of produced water from petroleum operations is vast, only a small fraction of it is reused or turned into potable water, for example, because of the lack of technologies to remove both dissolved and suspended solids at a significant throughput. This project shows that mesofluidic inline separators coupled with a commercial dissolved solids removal technology (RO) are positioned to do exactly that. Mesofluidic inline separators fit within commercial piping and are tunable for particle sizes of interest as described below. Indeed, mesofluidic inline separators have remarkably smaller footprints than competing filtration technologies and are easily transportable from jobsite to jobsite. This technology has no moving parts so that solids removal can be accomplished at much lower operating cost.

Summary of Research Results

Table 2. Summary of Milestones and Key Results

Milestone/Deliverable	Description/Key Results	Date Complete
1. Complete APEX/PNNL contract	Contract completed	FY22 Q1
2. Design & build mesofluidic inline separator	Separator physically realized	FY23 Q4
3. CFD model implemented	Presentation of model results	FY24 Q1
4. Test mesofluidic inline separator	Separator tested; letter report	FY24 Q2
5. Prepare manuscript	Manuscript PNNL approved	FY24 Q3
6. Prepare manufacturing licensing	License opportunity marketed	FY24 Q3

Highlights from milestones 2-4 are described in greater detail herein.

Design and Build Mesofluidic Inline Separator

PNNL explored first-of-a-kind ceramic mesofluidic separators to enhance produced water treatment. This work evaluated whether ceramic 3D printing may be used to create ceramic mesofluidic separators, which should be more mechanically robust than plastic (Pease, et al., 2022) but might be less expensive than metal (Burns, et al., 2021). A stated purpose of this effort for 3D printing was to evaluate the hypothesis that *ceramic 3D printing costs less with the same quality*. This hypothesis answers the question, "Can CoorsTek, Bosch, etc. print cost effectively?" Over the course of this work, PNNL engaged with three 3D printing companies (including CoorsTek and Bosch). The one that was most successful viz-a-viz our requests/designs (which have tight tolerances) has been Kyocera. Figure 1 shows test prints that vary the pin diameter and the number of supports. These results opened the opportunity to produce separators that separate particles of ~50 microns, a key size for flow streams that feed reverse osmosis systems, for example. Further work focused on the 16 micron separator as that will be able to remove an even larger fraction of particulate from produced water streams.

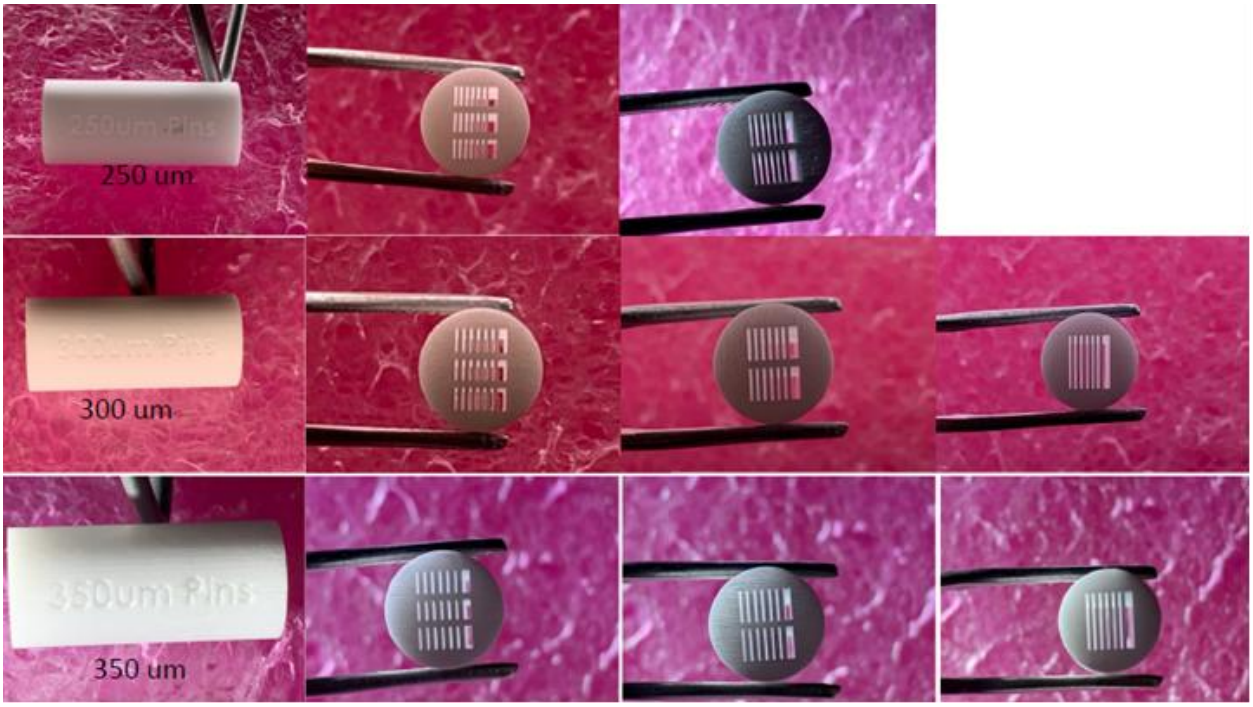

Figure 1. Test prints that vary the pin diameter and the number of supports.

Ceramic separators consisted of three types of parts: an entry piece, an exit piece, and one or more connective “pucks”. The current design requires at least 8 pucks. Kyocera showed success printing the entry and exit pieces in ceramic. However, the pucks for the 16-micron separator were challenging. Some appear suitable and others do not. Please note the inconsistent diameter of the pins and some of the pins are broken.

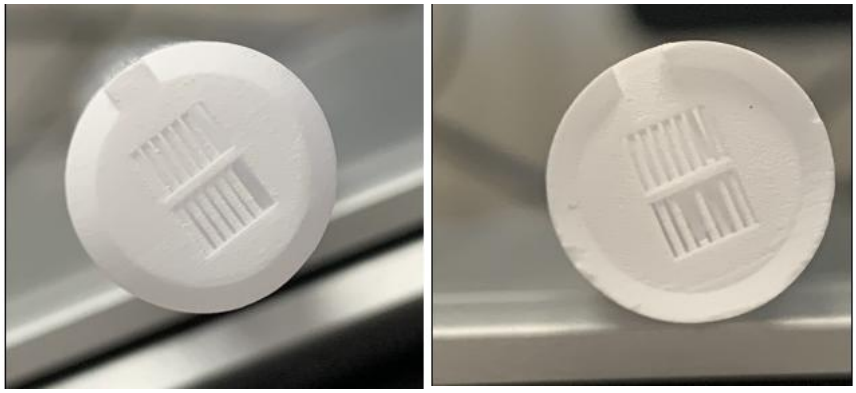

Figure 2. Images of the ends of test prints.

In net, a ceramic mesofluidic separator consisting of three types of parts: an entry piece, an exit piece, and multiple connective “pucks” was printed as promised. However, the 3D printed puck remains challenged. Figure 3 shows computed tomography of the inside of two of the pucks (labeled C and D) that had the best outside print of the most recent printing batch. The images present views of each puck from two directions (parallel and perpendicular to the pins). These images show that significant fractions of the pins are missing or out of place. If even a few of the pins are out of place the puck is defective and will not perform the desired separation. Taken together these printing errors indicate that ceramic printing is not yet able to produce the devices at the dimensions needed to separate particles at the 16-micron cutoff level. The technology

continues to advance. Parts that were challenging to produce yesterday may potentially be produced with ease tomorrow.

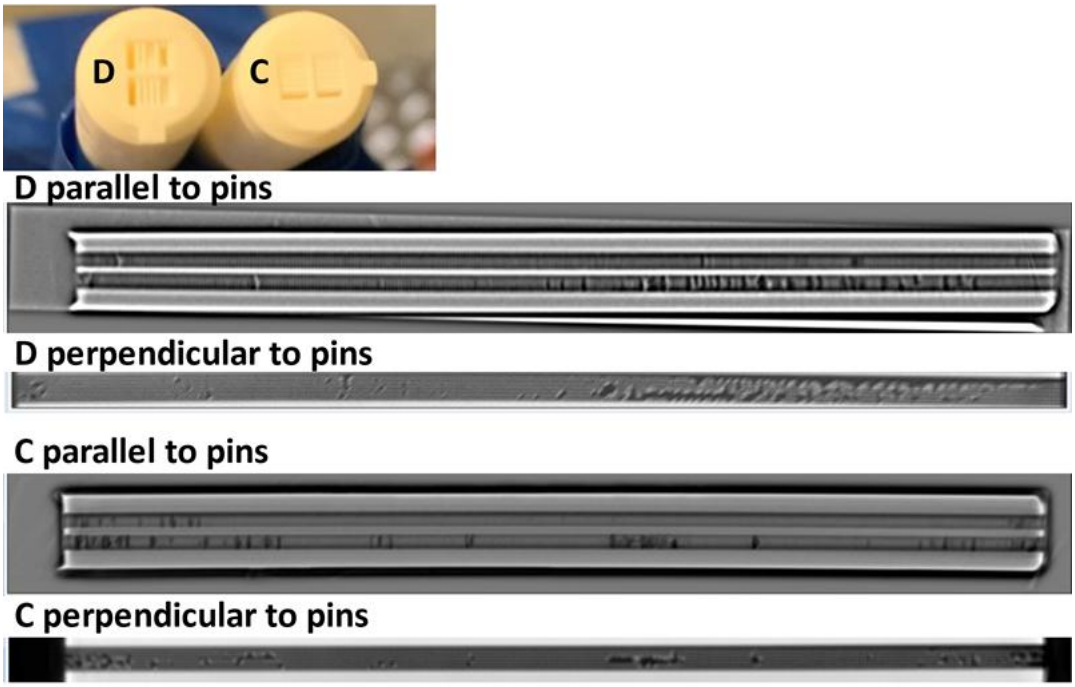

Figure 3. Images of two rods from two perpendicular perspectives. The design called for pins with a diameter of 300 micron and a gap of 225 microns. These computed tomography (CT) images are FFT transforms in which missing pins show up as dark patches.

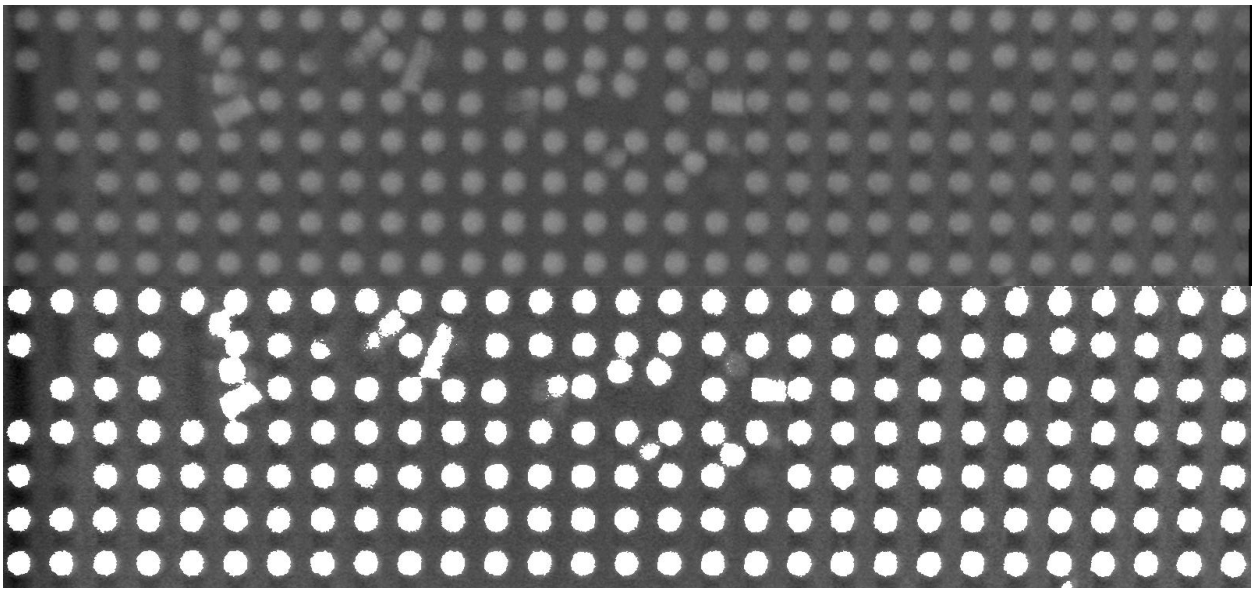

Figure 4. Images of pins. The bottom CT image is a contrast enhanced version of the top CT image.

PNNL performed a head-to-head comparison of the costs of 3D printing from the three materials: ceramic, metal, and plastic. Table 3 shows the cost comparison. It shows that for the smaller sizes (e.g., a 16 micron separator), plastic printing is not really an option both because

300-micron diameter pins cannot yet be well printed and because the plastic is not as durable due to the loss of plasticizers. Although both ceramic and metal should maintain good durability, the cost difference between the two is significant. The ceramic printing costs remain nearly an order of magnitude higher than the costs of metal printing. However, as shown above the device cannot be printed reliably. Therefore, ceramic printing is not cost effective relative to metal. Remaining efforts as part of this effort will use metal or plastic.

Table 3. Comparable Costs of Mesofluidic Devices

Material	Cost	Durability
Ceramic	$18k-$46k	Acceptable
Metal	~$2.5k	Acceptable
Plastic	Cannot print this small so far	Short
Note: 16-micron target. Success rates of 50% for ceramic 3D printing assumed. The relative prices are likely to change as each technology matures.		

To proceed with subsequent milestones, ceramic-resin composite separators were printed in-house. These were successfully printed with a 50-micron particle separation target.

Figure 5. Image of the polymer mesofluidic device printed in white resin in 8 sections.

Analytical-Computational Fluid Dynamics (CFD) Framework

Please see Appendix A for a manuscript describing these accomplishments and key successes.

Test of Mesofluidic Inline Separator Coupling with Reverse Osmosis

Please see Appendix B for a manuscript describing these accomplishments and key successes.

References

Leonard F. Pease, Nathan R. Philips, Jason Serkowski, Timothy G. Veldman, Michael J. Minette, Carolyn A. Burns, Industrial Scale Mesofluidic Particle Separation, Chemical Engineering and Processing – Process Intensification 173 (2022) 108795.

Carolyn A. Burns, Timothy G. Veldman, Jason Serkowski, Richard C. Daniel, Xiao-Ying Yu, Michael J. Minette, Leonard F. Pease, Mesofluidic Separation versus Dead-end Filtration, Separation and Purification Technology 254 (2021) 117256.

Subject Inventions

No new subject inventions were created as part of this Technology Commercialization Fund project and corresponding CRADA.

Products

Two manuscripts describing the modeling and coupled experiments have been prepared as shown in Appendix A and Appendix B.

Appendix A: Analytical-Computational Fluid Dynamics (CFD) Framework

Proceedings of the ASME 2025
International Mechanical Engineering Congress and Exhibition
IMECE2025
November 16-20, 2025, Memphis, TN, USA
IMECE2025-158876

MESOFLUIDIC SEPARATOR FLOW FIELDS AND SPLIT FRACTIONS

Sarah R. Suffield, Carolyn A. Burns, Judith A. Bamberger, Michael J. Minette, and Leonard F. Pease
Pacific Northwest National Laboratory
Richland, Washington, USA

ABSTRACT

Here we evaluate the flow fields in mesofluidic separators to determine the fluid split fraction between the two exits. Similar to microfluidic bump arrays, the flow fields around the array of pins drive particles of sufficient size to one side of the device leaving one exit depleted in particles and the other exit enriched in particles. However, mesofluidic separators differ from microfluidic bump arrays at least because they can accommodate much larger particles and because they can operate at much higher flowrates.

The higher flowrates affect the flow fields within the device leading to vorticity and turbulence. In most flow situations, turbulence and vorticities would smooth out particle concentration profiles, canceling the influence of the bump arrays. However, experiments show that there is still a separation under these conditions beyond that from gravity (a surprising and unexpected result), and the onset of turbulence within these devices is unclear (i.e., do the pins induce or reduce turbulence).

The larger particles require an exit large enough to permit these larger particles to leave without clogging the device. This pathway provides a lower resistance pathway for these particles. How much of the flow proceeds through this pathway as opposed to the higher resistance pathway of the bump array remains unclear. A typical rule of thumb, suggesting that the area available to the exiting flow determines the exiting volumetric flowrate, fails because the resistance to the flow governs; but, semi-quantitative guidance on how to estimate these exiting flowrates has remained elusive.

Here we use a combination of analytical and computational models to evaluate the onset of turbulence with mesofluidic devices, determine the fraction of flow that exits through the express lane, and estimate pressure versus flowrate curves. Analytical expressions for the onset of turbulence and split fractions based on fluid resistance are determined. Further, we show that vortices form on one edge of the pins before the other due to the angle of the pins that breaks flow symmetry.

Keywords: slurry, solids removal, deterministic lateral displacement (DLD), bump arrays

NOMENCLATURE

A_p	cross-sectional area of permeate
A_x	cross-sectional area of express lane ($=s_x s_h$)
a_1-a_3	coefficients
b_1-b_4	coefficients
D	hydraulic diameter of device (based on $2r$ if circular or s_h if square),
D_p	hydraulic diameter of the permeate
d_p	pin diameter
D_x	hydraulic diameter of the express lane
f_D	Darcy friction factor through the permeate
f_p	friction factor through the pin array
f_x	Darcy friction factor of express lane
L	length of the express lane adjacent to the pin array.
N_L	number of pins (or number of rows) in the direction of flow
P_D	perimeter of device ($2\pi r$ if circular or $4s_h$ if square),
P_p	perimeter of permeate
P_x	perimeter of express lane
Q_f	volumetric flowrates of the feed
Q_p	volumetric flowrates of the permeate
Q_x	volumetric flowrates of the express lane
r	radius of the cross section
Re_f	Reynolds number of feed
Re_p	Reynolds number of permeate
Re_x	Reynolds number of express lane
S	permeate flowrate split fraction
s	segment length corresponding to the edge of the express lane
S_{cc}	center-to-center distance between pins in a row
s_h	length of the side of a square channel (s_h and s_x define the cross section of the express lane)s_x length of the express lane
V_f	average velocity of feed
V_p	superficial velocity of the permeate
$V_{p,max}$	maximum fluid velocity through the permeate portion of the device
V_x	velocity through the express lane

Greek Letters

β	1 for aligned and 4 for staggered
ΔP	pressure drop
ε	surface roughness
θ	angle defined from the circular center by the isosceles triangle with two sides of length r and one side of length s
μ	dynamic viscosity of the slurry or fluid
ν	the slurry or fluid kinematic viscosity
ρ	slurry or fluid density
ϕ	angle of the pins with respect to the sidewall in degrees
χ	constant

Subscripts

f	feed
p	permeate
x	express lane

INTRODUCTION

Mesofluidic separators are like microfluidic bump arrays with at least two key differences. Microfluidic bump arrays were first reported by Huang, et al., [1] as a means of separating particles by size (see Fig. 1). Inglis, et al., [2] provided a quantitative model to predict the performance of these devices specifically under laminar flow conditions (their formulas become increasingly inaccurate outside of the laminar range, which affect the structuring of the array of pins that drives separation [3, 4]). The essential feature of these devices is an array of pins, the centers of which form a non-zero angle with the sidewall. This angle breaks symmetry such that each pin in at least a pair of downstream rows provides a distinct stagnation streamline. These stagnation streamlines form the boundaries of flow channels. If the distance between the edge of pin and the nearest stagnation streamline is smaller than the radius of a particle, that particle must move away from the first pin into the next adjacent flow channel.

Mesofluidic separators challenge this model in two very specific ways. First, mesofluidic separators often operate at significantly higher flowrates than microfluidic systems [5-7]. The higher flowrates affect the flow fields within the device leading to vorticity and turbulence, which typically cancel stagnation streamline arguments. For this reason, authors historically have limited their analyses of microfluidic bump arrays to laminar conditions. In most flow situations, turbulence and vorticities would smooth out particle concentration profiles, canceling the influence of the bump arrays. Unexpectedly, experiments show that there is still a separation under these conditions beyond that from gravity [5], and the onset of turbulence within these devices is unclear (i.e., do the pins induce or reduce turbulence?). Therefore, a key question for modeling efforts is to determine the flow regimes within mesofluidic separators. This would be a relatively simple effort in the absence of the pins. In that case, the onset of turbulence corresponds to a conduit Reynolds number of ~1800. However, the presence of pins adds wrinkles to this picture. At the edge of a pin, the velocity goes to zero due to a no-slip condition with peak flow between the pins. As the flow leaves a row of pins it spreads out only to converge again as the next row of pins blocks a portion of the flow pathway. This sets up a periodic convergence as flow approaches a row of pins and divergence as flow leaves a row of pins. The onset of turbulence is known to be delayed (meaning it occurs at higher Reynolds numbers, e.g., >1800) in convergent flow and to be accelerated (meaning it occurs at lower Reynolds numbers, e.g., <1800) in divergent flow. The angle of the pins may also be influential but has not been explored previously. Dincau, et al., have explored flow conditions up to, but not including the Reynolds number, where vortex shedding becomes important and found that the particle size cutoff changes with flowrate [4]. Flowrates in the vortex shedding regime and higher have not been reported from a theoretical or modeling perspective.

The second difference between industrially relevant mesofluidic devices and microfluidic bump arrays is that the former are tailored to fit within pipes or conduits in contrast to most microfluidic arrays that are designed so that edge effects become unimportant (e.g., by including extra arrays pins between the particle flow pathways and the walls that serve no separation purpose but substantially increasing the cross section of these devices—additions that would require much larger flows in larger-scale industrial applications). These edges induce fluid interactions between the walls of the pins and device walls and the particles and fluid that transport between them. For example, larger particles require an exit large enough to permit these larger particles to leave without clogging the device. This pathway provides a lower resistance pathway for these particles. How much of the flow proceeds through this pathway as opposed to the higher resistance pathway of the bump array remains unclear. A typical rule of thumb suggesting that the area available to the exiting flow determines the exiting volumetric flowrate fails because the resistance to the flow govern, but semi-quantitative guidance on how to estimate these exiting flowrates has remained elusive.

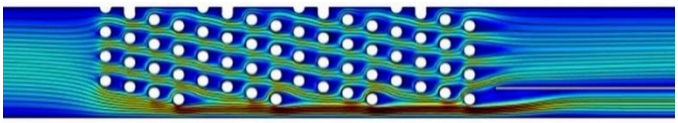

FIGURE 1. IMAGE OF FLOW PROFILE IN A MESOFLUIDIC INLINE SEPARATOR WITH RED INDICATING FASTER VELOCITIES AND BLUE INDICATING SLOW VELOCITIES. THE EXPRESS LANE HAS THE HIGHEST FLOWRATES, BECAUSE IT HAS THE LEAST RESISTANCE EVEN THOUGH IT HAS A SMALL CROSS-SECTIONAL AREA. NOTE THAT THERE IS AN INTERNAL SPLIT FRACTION (ONLY WITHIN THE PIN ARRAY) AND AN EXTERNAL SPLIT FRACTION (ACROSS THE WHOLE DEVICE) AS THE FLOW CAN REBALANCE BETWEEN THE END OF THE BUMP ARRAY AND THE EXITS BASED, AT LEAST PARTIALLY, ON THE PRESSURE DROPS.

In the remainder of this paper, we first model the fluid mechanics of these mesofluidic separators. We then describe the results for pressure drop and split fraction as a function of

flowrate using a combination of analytical and computational fluid dynamics. We conclude with insights into the onset of turbulence within these devices and the influence of asymmetry.

MODEL AND METHODS

Here we present a model that uses both an analytical framework with insight from computational fluid dynamics (CFD) to understand the pressure drop, the split fractions, and the role of turbulence in these devices. We represent this system as though it has two resistances in parallel. One is the friction through the pin array and one is the friction associated with the sidewalls. We treat flow through the pin array and the express lane as separate flow channels, recognizing that they are physically in "fluid communication". For the express lane, we consider it to be an open channel with a hydraulic diameter defined by the edges of the pins and the side walls. Because this definition of the express lane varies somewhat with position (the pins are at a finite angle with respect to the wall), this model permits exploration of the minimum, maximum, and median/average express lane position.

For the express lane, we use the hydraulic diameter, D_x, which is

$$D_x = \frac{4A_x}{P_x}, \tag{1}$$

where P_x is the perimeter and A_x is the cross-sectional area. Our cross sections are typically either rectangular or circular. For rectangular cross sections,

$$D_x = \frac{2s_h s_x}{s_h + s_x}, \tag{2}$$

where s_x is the length of the express lane and s_h is the length of the side of the rectangle completing the cross-sectional area ($=s_x s_h$). For a circular cross section, the express lane has a flat edge and a curved edge. Then

$$D_x = 2r\frac{\theta - \sin\theta}{\theta + 2\sin\left(\frac{\theta}{2}\right)}, \tag{3}$$

constrained by

$$\frac{s}{2} = r\sin\left(\frac{\theta}{2}\right), \tag{4}$$

where r is the radius of the cross section, θ is the angle defined from the circular center by the isosceles triangle with two sides of length r and one side of length s, and s is the segment length corresponding to the edge of the express lane. For the Reynolds number, Re_x, if turbulent, roughness may then be used to determine the relationship between pressure drop and flow. The Darcy friction factor, f_x, expressions for the express lane for laminar and turbulent flow (see Afzal 2013 Eq. 41 [8]) are given, respectively, as

$$f_x = \frac{64}{Re_x}, \tag{5}$$

$$\frac{1}{\sqrt{f_D}} = -2\,log_{10}\left[\frac{\frac{\varepsilon}{D}}{3.7}\left(1 - Exp\left[-\frac{Re_x\frac{\varepsilon}{D}\sqrt{f_D}}{2.83*26}\right]\right) + \frac{2.51}{Re_x\sqrt{f_D}}\right] \tag{6}$$

where f_D is the Darcy friction factor in the permeate, ε is the surface roughness, and D is the hydraulic diameter with Reynolds number for the express lane

$$Re_x = \frac{\rho V_x D_x}{\mu} = \frac{4Q_x}{\nu P_x}, \tag{7}$$

where this V_x is the superficial velocity through the express lane adjacent to the pins, D_x is the hydraulic diameter of the express lane, ρ is the slurry or fluid density, μ is the dynamic viscosity of the slurry or fluid, and ν is the slurry or fluid kinematic viscosity. The Darcy-Weisbach expression gives the pressure drop, ΔP,

$$\Delta P = \frac{f_x L}{2D_x {A_x}^2}\rho {Q_x}^2, \tag{8}$$

where L is the length of the express lane adjacent to the pin array, and Q_x is the volumetric flowrate of the express lane.

For the pin array, we consider two expressions for the pressure drop. The first one derives from expressions for flow around tubes in a bank of tubes, similar to the pin array. Here the pin array has an angle with respect to the sidewall, which is typically but not always small. Incropera, et al. [9], give expressions for aligned and staggered arrangements of tubes, neither of which are perfect for mesofluidic devices. For small or shallow angles, the aligned arrangement is most relevant, though the development below incorporates a staggered arrangement. In either case, the pressure drop, ΔP, is then

$$\Delta P = N_L \chi \left(\frac{\rho {V_{p,max}}^2}{2}\right) f_p, \tag{9}$$

where N_L is number of pins (or number of rows) in the direction of flow, and χ is a constant, and friction factor in the permeate, f_p, is given in Figs. 7.13-7.14 in Incropera, et al. [9]

$$V_{p,max} = \begin{cases} \frac{S_{cc}}{S_{cc} - d_p} V_p & \text{aligned} \\ \frac{S_{cc}}{2(S_{cc} - d_p)} V_p & \text{staggered} \end{cases}, \tag{10}$$

where V_p is the superficial velocity of the permeate, S_{cc} is the center-to-center distance between pins in a row, and d_p is the pin diameter. Then

$$\Delta P = \frac{N_L \chi f_p}{2\beta {A_p}^2}\left(\frac{S_{cc}}{S_{cc} - d_p}\right)^2 \rho {Q_p}^2, \tag{11}$$

where A_p is the cross sectional area of the permeate, β is 1 for aligned and 4 for staggered. Because the pin array typically has only a slight angle with respect to the sidewall, the pins are often nearly aligned and β does not differ substantially from ~1. In

this formulation, the pressure drop increases quadratically with flow, which was observed in Pease, et al. [5].

By conservation of mass,

$$\rho Q_f = \rho Q_x + \rho Q_p, \tag{12}$$

where Q_f, Q_x, and Q_p are the volumetric flowrates of the feed, express lane, and permeate, respectively. The inclusion of density serves as a reminder that, although constant density is assumed to be approximately commensurate with measurements to date, the density could vary among the three streams in ways not captured below.

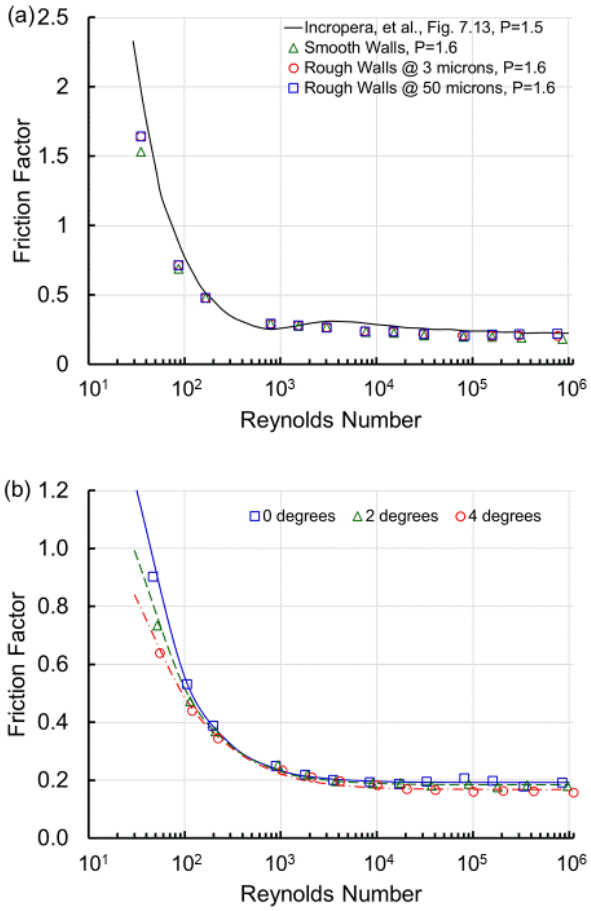

FIGURE 2. THE FRICTION FACTOR, f_p, THROUGH THE PERMEATE BASED ON PEAK FLOWRATE BETWEEN PINS VERSUS THE REYNOLDS NUMBER OF THE DEVICE BASED ON THE HIGHEST FLOWRATE, $V_{p,max}$ AS A FUNCTION OF THE ANGLE OF THE PINS WITH RESPECT TO THE SIDEWALL GENERATED FROM STAR-CCM+ RESULTS.

The permeate flowrate split fraction, S, may be defined as

$$S \equiv \frac{Q_p}{Q_f} = \frac{Q_f - Q_x}{Q_f}. \tag{13}$$

We may now combine the pressure drop expressions and conservation of mass so that

$$S = \left[1 + \sqrt{\frac{f_p}{f_x}\frac{\chi}{\beta}\frac{N_L D_x}{L}}\frac{A_x}{A_p}\left(\frac{S_{cc}}{S_{cc}-d_p}\right)\right]^{-1}. \tag{14}$$

where A_p is the cross-sectional area of the permeate. Essentially, the flowrate split depends on one dimensionless group that must range from zero to one. This solution is highly dependent on geometry, though flow remains a contributor via the friction factors.

An essential variable missing in this model is the friction factor through the pin array of the permeate, f_p. Beale [10] (see his Eq. 11) provides a power law approximation with coefficients a_1-a_3

$$f_p = a_1\left(a_2 + \frac{1}{Re_p}\right)^{a_3}\left(b_1 Exp\left(-10^{-b_2}Re_p\right) - \frac{b_3}{Re_p} + b_4\right) \tag{15}$$

with a final factor included here that accounts for the offset in angle with coefficients b_1-b_4 and Re_p is the Reynolds number of the permeate. This approximation does not directly address the influence of surface roughness, because surface roughness was not given explicitly by Beale [10] and Fig. 2a does not suggest a strong influence for surface roughness so long as there is some roughness. Figure 2 shows the friction factor as a function of a Reynolds number from the CFD model compared to data extracted from Figs. 7.13-7.14 in Incropera, et al. [9]. The figure shows some variation with respect to angle that is captured in the equations developed above and a modest contribution from friction. The CFD model results are close to those presented in Incropera, et al., [9]. The coefficients a_1 and a_3 were fit from Table 1 of Beale [10] and a_2 was corrected based on the value of Fig. 7.13 of Incropera, et al., [9] at Re_p=1.0·10^6 to find

$$\begin{aligned} a_1 &= 586.58\left(\frac{S_{cc}}{d_p}\right)^{-4.605} \\ a_2 &= -0.004205\left(\frac{S_{cc}}{d_p}\right)^2 + 0.01622\left(\frac{S_{cc}}{d_p}\right) - 0.01235 \\ a_3 &= -0.2667\left(\frac{S_{cc}}{d_p}\right)^2 + 0.6613\left(\frac{S_{cc}}{d_p}\right) + 0.604. \end{aligned} \tag{16}$$

The coefficients b_1-b_4 were determined from the CFD as

$$\begin{aligned} b_1 &= 0.004345\phi^2 + 0.01162\phi \\ b_2 &= -0.005368\phi + 3.538 \\ b_3 &= -0.2933\phi^2 + 3.501\phi \\ b_4 &= -0.005528\phi^2 - 0.009157\phi + 1 \end{aligned} \tag{17}$$

where ϕ is the angle of the pins with respect to the sidewall in degrees.[1] Additional refinement of b_2 may increase precision. The Reynolds number of the permeate is given as

$$Re_p = \frac{\rho V_p D_p}{\mu} = \frac{4Q_p}{\nu P_p} \quad (18)$$

and

$$D_p = \frac{4A_p}{P_p}, \quad (19)$$

where P_p is the perimeter and A_p is the cross-sectional area. Our cross sections are typically either rectangular or circular. For square cross sections,

$$D_p = \frac{2s_h(s_h - s_x)}{2s_h - s_x}, \quad (20)$$

where D_p is the hydraulic diameter of the permeate, s_x is the length of the express lane and s_h is the length of the side of the rectangle completing the cross-sectional area ($=s_x s_h$). For a circular cross section, the express lane has a flat edge and a curved edge. Then for the permeate

$$D_p = 2r\frac{2\pi - \theta}{2\pi - \theta + 2sin\left(\frac{\theta}{2}\right)}, \quad (21)$$

constrained by Eq. 4.

The Reynolds numbers are related via

$$Re_f = \frac{\rho V_f D}{\mu} = \frac{4Q_f}{\nu P_D}, \quad (22)$$

$$Re_x = Re_D(1 - S)\frac{P_D}{P_x}, \quad (23)$$

$$Re_p = Re_D S\frac{P_D}{P_p}, \quad (24)$$

where D is the hydraulic diameter of the device ($2r$ if circular or s_h if square), P_D is the perimeter of the device ($2\pi r$ if circular or $4s_h$ if square), and V_f is the average velocity of the feed.

A Reynolds-averaged Navier-Stokes (RANS) model with a k–ε turbulence flow model was applied to the fluid region, which was assumed to be water. Flow across the tube bundle was driven by a velocity inlet upstream of the bundle, and the boundary downstream of the bundle was specified as an outlet. Along each wall boundary, including the boundary around each pin, orthogonal prismatic cell layers were applied to the mesh to improve the accuracy of the flow solution near these surfaces.

[1] These correlations were generated from the following coefficients fit to CFD data for S_{cc}/d_p=1.6.

CFD has been used to develop a quantitative expression to improve analytical predictions. Specifically, we developed a CFD model of an inline tube bundle, similar to textbook correlations for friction factor as a function of Reynolds number, albeit including the angle of asymmetry. The commercial CFD software STAR-CCM+ was used to develop the inline tube bundle model. The model included a single fluid region that flowed through a 7x7 array of tubes (Fig. 3). Each tube had a diameter of 0.5 mm, and the orientation of the tube array was varied from an inline configuration with a 0 degree tilt to a 4 degree tilt orientation (see Fig. 3).

We also conducted an X-ray computed tomography (XCT) scan to image the inside of the mesofluidic device. XCT image scanning was conducted using a Nikon X-Tek/Metris XTH 320/225 kV instrument (Nikon Metrology, Belmont, CA, USA) at 105 kV and 325 μA, with a 0.5-mm Cu filter reducing beam hardening artifacts. During scans, each sample core was rotated continuously with brief stops for projection collection, totaling 3142 projections over a 360˚ rotation, capturing two frames per projection with 500 ms exposure time for each frame. This yielded a voxel size of 7.4 μm and a spatial resolution of ~15 μm. Images were reconstructed into 3D volumes with CT Pro 3D (version XT 2.2, Nikon Metrology, Inc).

RESULTS AND DISCUSSION

In this paper, we describe three key aspects of mesofluidic separator performance. First, we use the model described above to predict the pressure drop versus flowrate. Second, we predict the split fraction between the permeate and the express lane. We note that the internal split fraction modeled here may differ meaningfully from the split fraction that develops after the flows exit the pin arrays due to system pressure drops (e.g., a lower pressure drop permeate flow may pull some express lane flow within the device into the permeate exit). Third, we evaluate the velocity profiles through the pins in consideration of the onset of turbulence.

An essential outcome of the model above is the relationship between the pressure drop through the device and the flowrate. Essential to that outcome is the development of expressions to represent friction within the pin array that account for its tilt with respect to the sidewalls. Fig. 3 shows the resulting velocity plots for 0 and 4 degrees of tilt. Notably, after flow is established, the velocity at the bottom of a pin (see Fig. 3) is higher than the velocity around the top of a pin.

Figure 4 shows the pressure drop versus the flowrate through the mesofluidic device using a fluid interconnect model that pairs a nearly aligned (small angle) tube model representing the pin array with an open channel model representing the express lane portion of the flow channel. The agreement with experimental data is quite reasonable with best agreement

Angle	a_1	a_2	a_3
0 degrees	16.88	0.003576	0.7943
2 degrees	7.663	0.002294	0.6131
4 degrees	4.339	0.001288	0.4884

between modeling and experiment acknowledging that the pin diameters of as-built devices may be larger in diameter than as-designed devices. The red data was taken early in a several week campaign and the blue data was take late in the campaign. Both data sets evaluate the flow of water through the device, though all the other tests during that time employed concentrated simulants with particles that may have accumulated on the surface. Indeed, the pins were discolored by the time of taking of the second data set in blue suggesting that the pins were indeed coated with a thin layer of simulant particles. The two model curves differ in that the upper dashed curve corresponds to a pin diameter that is 0.02 mm larger in radius than the lower solid curve, which is commensurate with the 4-30 micron (mode-95 percentile) particles used in those experiments.

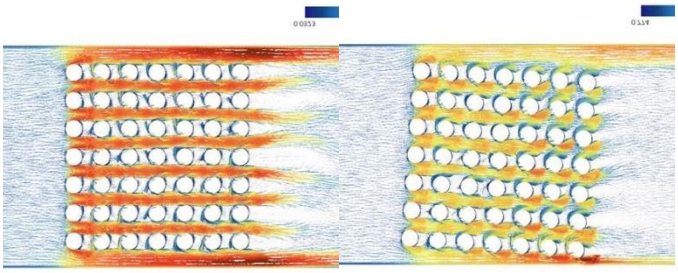

(a) (b)

FIGURE 3. VELOCITY VECTOR PLOTS FOR (a) 0 DEGREE AND (b) 4 DEGREE ANGLE OF THE PINS WITH RESPECT TO THEIR SIDEWALLS. VELOCITIES ABOVE AND BELOW A POST DIFFER WHEN SYMMETRY IS BROKEN.

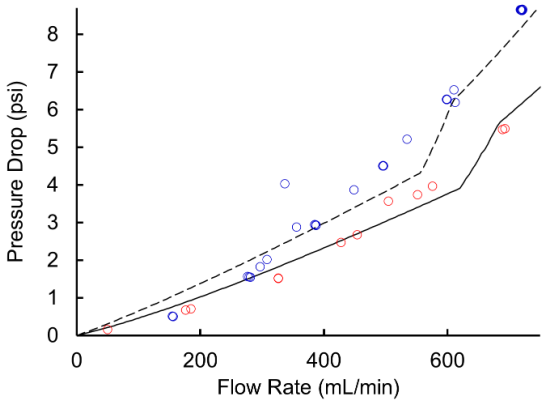

FIGURE 4. PRESSURE DROP VERSUS FLOWRATE.

A key metric of performance of mesofluidic separators is the fluid split fraction that goes through bump array or out the permeate exit. The remaining flow goes to the express lane. In many cases, increasing the split fraction, or the product of the split fraction with the entering flowrate, are important to downstream applications. In the course of modeling, two split fractions become important: the internal split fraction and the external split fraction. The external split fraction is the split fraction as measured on the inlet and outlet. This split fraction is strongly influenced by inlet and outlet pressures. The internal split fraction is the split fraction as measured within the device. The internal split fraction to the permeate is important because it influences the external split fraction and because the particles migrate relative to this split fraction.

Our modeling framework explored the split fraction as a function of Reynolds number based on feed conditions and as a function of position down the separator channel. Figure 5 shows that the split fraction is a function of the feed Reynolds number. As the flowrate increases, more flow goes through the express lane than the permeate channel. The split fraction is controlled in part by the ratio of the friction factor in the permeate to the friction factor in the express lane. When this ratio increases there is less resistance to flow through the express lane, so more flow goes through the express lane than the permeate.

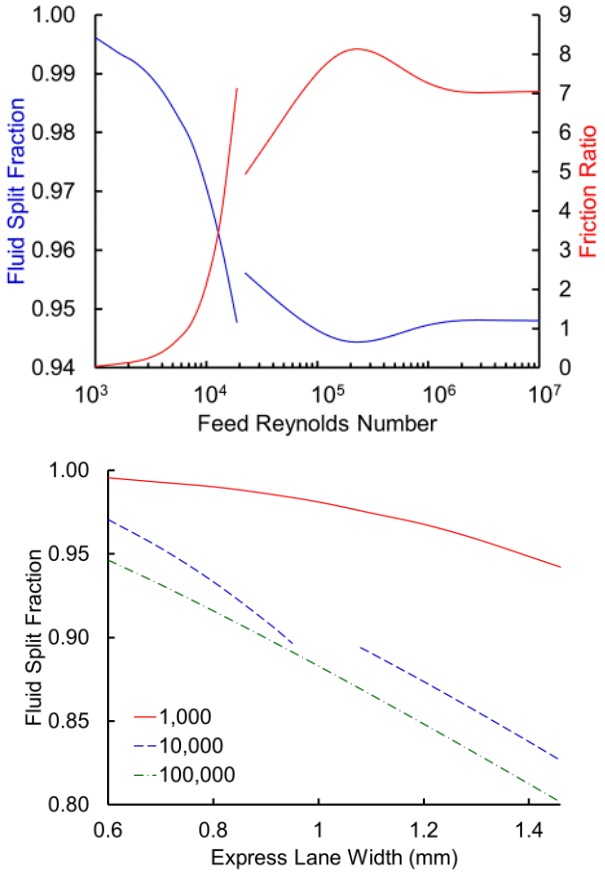

FIGURE 5. (TOP) FLUID SPLIT FRACTION (BLUE), *S*, AND FRICTION RATIO (RED), f_p/f_x, VERSUS FEED REYNOLDS NUMBER, Re_f, BASED ON THE CHANNEL OPENING WITH DIMENSIONS BASED ON THE DEVICE REPORTED IN BURNS, ET AL. (2021). (BOTTOM) FLUID SPLIT FRACTION TO THE PERMEATE VERSUS EXPRESS LANE WIDTH. IN BOTH PANELS, THE DISJOINT IN THE CURVES OCCURS WHEN THE EXPRESS LANE TRANSITIONS BETWEEN LAMINAR AND TURBULENT FLOW (E.G., Re_x=1800).

Further, the internal split fraction varies with position down the channel. Figure 6 shows that the pins change position, albeit gradually, down the channel. The express line narrows (flow from right) and then widens as a column of pins ends. Figure 5

shows that the split fraction to the permeate decreases as the express lane widens. Remarkably, the variation in the internal split fraction can be meaningful.

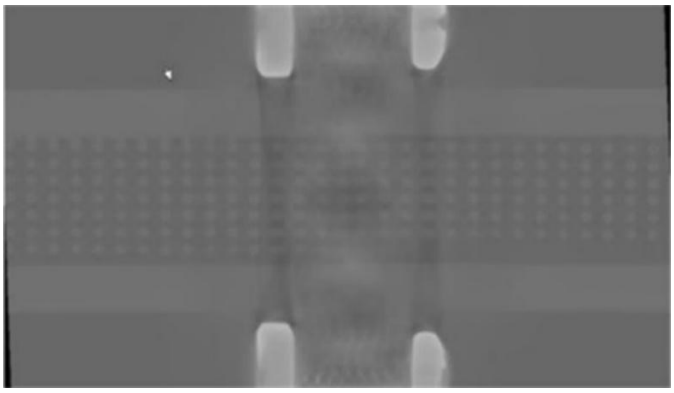

FIGURE 6. CT IMAGE OF THE PINS SHOWING THAT THE EXPRESS LANE PINS VARY AS A FUNCTION OF POSITION IN A MESOFLUIDIC DEVICE JOINED BY SCREWS. THE SPLIT FRACTION TO THE PERMEATE WILL INCREASE FROM LEFT TO RIGHT BUT THEN DROP AS THE NEW ROW OF PINS DIVIDES THE EXPRESS LANE. *THIS IS THE FIRST IMAGE OF THE AS-BUILT INTERNALS OF A MESOFLUIDIC DEVICE.*

A key question is how turbulence affects the performance of mesofluidic separators. These separators function based on the interaction of fluid flow with pins. The pins are angled with respect to the sidewall of the channel. On the upstream side of every pin the fluid divides with some of the fluid going to one side of the pin and some of the fluid going to the other side of the pin. The point at which this division occurs is called the stagnation point and the streamline that anchors to this position is called the stagnation streamline. These streamlines form flow channels that govern the separation. Small particles stay within a flow channel, whereas large particles consecutively bump from one flow channel into the next as they pass each row of pins. This description suffices (in the absence of edge effects) under laminar conditions. Others have shown that, as the Reynolds number increases, vortices begin to form [4], but what happens at higher Reynolds numbers has not previously been explored, though separation at higher Reynolds numbers have been shown at industrial scale flowrates.

The role of turbulence boils down to the question of which flow regimes govern within the region defined by the pins in the mesofluidic separator. Determining the flow regime in the entrance and exit regions is straightforward. However, the flow regime within the pin region has been less obvious. The velocity between the pins must be elevated because of the decreased cross-sectional area available for flow, suggesting an earlier transition to turbulence. In contrast, the pins may serve to laminarize the flow, and screens similar in local geometry to these pin arrays are used to laminarize flow in wind tunnels, for example.

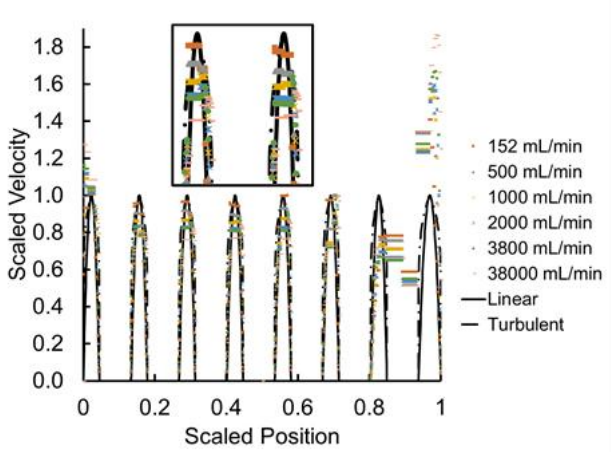

FIGURE 7. SCALED VELOCITY VERSUS SCALED POSITION FOR DIFFERENT FLOWRATES FIT TO LAMINAR AND TURBULENT MODELS.

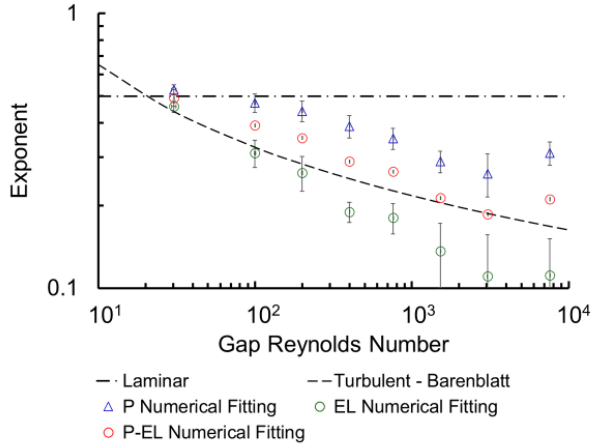

FIGURE 8. EXPONENTS FROM POWERLAW FITS VERSUS REYNOLDS NUMBER OF FLOW IN THE GAP BETWEEN PINS.

One means of determining the flow regime is to use computational fluid dynamics (CFD) to determine the velocity profiles in the average direction of flow along a transverse that is perpendicular to the channel sidewall and then determine if they adopt a parabolic profile, suggestive of a laminar flow regime, or a fractional power law (e.g., a $1/7^{th}$ power), suggestive of turbulent flow. Figure 7 shows these velocity profiles across a range of flowrates scaled with wall away from the express lane at 0 and the wall adjacent to the express lane at 1. Likewise, the velocity scales from zero where the pins are to 1 between the pins. The express lane has a higher velocity because it has more open space and, therefore, less resistance. The figure also shows the laminar model (a parabolic profile) and a turbulent model (here a $1/7^{th}$ power law). The inset shows that the CFD evaluated velocities fall between these two model velocity profiles. Comparing "ideal" profiles to the data from the CFD run shows that at the lowest flowrate the velocity profile is indeed parabolic but at the higher velocities the velocity profile departs from the parabolic profile. The large peak on the right of the plot

corresponds to the express lane. These profiles are approximately periodic and reminiscent of those of Giese, et al. [12] for flow through porous media, although the specifics of the geometry vary.

Although a transition between laminar and turbulent flow conditions at a distinct Reynolds number may arise under other flow conditions, Figure 8 shows a more gradual transition for these flow conditions. We fit the velocity profiles between ~0.2 to ~0.6 with curves to determine the exponent. Each half of the velocity profile was fit separately (i.e., the portion of the velocity profile on the permeate side, noted P, was fit separately from the velocity profile on the express lane side, noted EL). The figure below shows that the express lane halves have an exponent that decays as a function of the Reynolds number based on gap parameters (i.e., the width of the gap and the average velocity through the gap). The dashed line represents the exponential expression for open pipes by Barenblatt and Goldenfeld [11] (1995) under turbulent conditions. The halves of the velocity profile near the permeate side appear to follow the laminar condition to higher gap Reynolds numbers before beginning to decay. This suggests that the two halves of the velocity profile behave differently with turbulence somewhat depressed on the permeate side in contrast to the express lane side. These results have implications for the way that turbulent diffusion should affect the motion of particles through the separator.

CONCLUSIONS

In summary, we generated a model to evaluate the pressure drop and split fraction versus flowrate for mesofluidic devices. The model comprises an overall analytical framework informed by select CFD results. In this manner, the results are not limited to select instances dictated by CFD constraints but allow the model to capture and predict over a wide range of conditions, which benefits from the precision that CFD provides.

ACKNOWLEDGEMENTS

Pacific Northwest National Laboratory is a multiprogram national laboratory operated for the U.S. Department of Energy by Battelle Memorial Institute under Contract DE-AC05-76RLO 1830. Funding for this work was provided by the U.S. Department of Energy under Department of Energy Contract DE-AC05-76RL01830.

REFERENCES

[1] Huang, L.R., E.C. Cox, R.H. Austin, J.C. Sturm. 2004. Continuous particle separation through deterministic lateral displacement. Science, 304, 987–990. https://doi.org/10.1126/science.1094567.

[2] Inglis, D.W., J.A. Davis, R.H. Austin, J.C. Sturm. 2006. Critical Particle Size for Fractionation by Deterministic Lateral Displacement Lab Chip, 6, 655–658. https://doi.org/10.1039/B515371A.

[3] Pease L.F., J.E. Serkowski, T.G. Veldman, J. Williams, X.-Y. Yu, M.J. Minette, J.A. Bamberger, C.A. Burns. 2021. Can Bump Arrays Separate Particles from Turbulent Flows?. In Proceedings of the ASME 2021 Fluids Engineering Division Summer Meeting (FEDSM 2021), August 10-12, 2021, Virtual, Online, 3, FEDSM2021-67696, V003T08A024. New York, New York: ASME. https://doi.org/10.1115/FEDSM2021-67696.

[4] Dincau, B.M., A. Aghilinejad, T. Hammersley, X. Chen, J.-.H Kim. 2018. Deterministic lateral displacement (DLD) in the high Reynolds number regime: high-throughput and dynamic separation characteristics, Microfluid Nanofluidics 22, 59. https://doi.org/10.1007/s10404-018-2078-9.

[5] Pease, L.F., N.R. Philips, J. Serkowski, T.G. Veldman, M.J. Minette, C.A. Burns. 2022. Industrial Scale Mesofluidic Particle Separation, Chemical Engineering Processing – Process Intensification 173 (2022) 108795. https://doi.org/10.1016/j.cep.2022.108795.

[6] Pease, L.F. T.G. Veldman, J. Serkowski, N.R. Phillips, R.C. Daniel, M.J. Minette, X.Y. Yu, M.S. Fountain, C.A. Burns. 2020. Efficient Mesofluidic Separation of Large Particles in Nuclear Slurries, Waste Management Symposium 2020 Proceedings, Paper 20408.

[7] Burns C.A., T.G. Veldman, J. Serkowski, R.C. Daniel, X.-Y. Yu, M.J. Minette, L.F. Pease. 2021. Mesofluidic Separation versus Dead-end Filtration. Separation and Purification Technology, 254, 117256. https://doi.org/10.1016/j.seppur.2020.117256.

[8] Afzal, N., A. Seena, A. Bushra. 2013. Turbulent flow in a machine honed rough pipe for large Reynolds numbers: general roughness scaling laws. J. Hydro-Environ. Res. 7, 81-90. https://doi.org/10.1016/j.jher.2011.08.002.

[9] Incropera, F.P., D.P. DeWitt, T.L. Bergman, A.S. Lavine. 2007. Fundamentals of Heat Transfer. Sixth Edition. John Wiley & Sons, Hoboken, NJ.

[10] Beale, S.B. 2012. A Simple, Effective Viscosity Formulation for Turbulent Flow and Heat Transfer in Compact Heat Exchangers. Heat Transfer Engineering, 33, 4-11.

[11] Barenblatt, G.I. and N. Goldenfeld. 1995. Does fully developed turbulence exist? Reynolds number independence versus asymptotic covariance. Phys. Fluids 7, 2078-2082. https://doi.org/10.1063/1.868685.

[12] Giese, M., K. Rottschafer, D. Vortmeyer. 1998. Measured and modeled superficial flow profiles in packed beds with liquid flow. American Institute of Chemical Engineers Journal, 44, 484-490. https://doi.org/10.1002/aic.690440225.

Appendix B: Test of Mesofluidic Inline Separator Coupling with Reverse Osmosis

***Submitted to* the ASME 2026**
Fluids Engineering Division Summer Meeting
FEDSM2026
July 26-29, 2026, Bellevue, Washington

FEDSM2026-XXXXXX

PRODUCED WATER TREATMENT USING MESOFLUIDIC INLINE SEPARATION AND REVERSE OSMOSIS

Carolyn A. Burns, Stony T. Akins, Jason Serkowski, Chinmayee Subban,
Judith A. Bamberger, Michael J. Minette, Leonard F. Pease
Pacific Northwest National Laboratory
Richland, Washington, USA

ABSTRACT

Here we demonstrate the combination of mesofluidic inline separators and reverse osmosis to remove dissolved and nondissolved solids from produced water to drinking water concentrations. Mesofluidic inline separators have previously demonstrated selective particle separation by size in high bay environments, and reverse osmosis is a standard commercial approach to desalination. A unit operation upstream of the reverse osmosis membrane is essential to remove non-dissolved solids and oil droplets to protect this membrane. However, coupling these separators with reverse osmosis has not been explored previously.

Here we describe the first design, construction, and bench testing of coupled mesofluidic inline separators with reverse osmosis systems. We show that mesofluidic inline separators can increase the amount of solids that the system is subjected to before clogging by approximately an order of magnitude. Further, the produced water that enters the mesofluidic inline separator at ~5300 ppm emerges from the reverse osmosis membrane at ~80-360 ppm, well within the drinking water range.

These results comprise the first essential step in treating produced water using this combination of technologies, because suspended solids can clog downstream unit operations including reverse osmosis systems. The combination of technologies provides an important pathway for the treatment and reuse of produced water (e.g., for surface discharge, reusable water, agricultural water, industrial use water, potable water, etc.).

Keywords: slurry, solids removal, deterministic lateral displacement (DLD), bump arrays, water purification, produced water, brine, desalination, critical minerals, critical materials

INTRODUCTION

Mesofluidic inline separators represent an opportunity to remove a key barrier in the treatment of produced water: suspended solids that clog downstream operations. The US alone produces very large quantities of produced water each year, most of which is reinjected as a waste product [1]. The impact from treating and reusing even a fraction of this water is immense. Although the amount of produced water from petroleum operations is vast and some must be returned to rebalance geophysical stresses, only a small fraction of it is reused or turned into potable water due, for example, to the lack of cost competitive technologies to remove both dissolved and suspended solids at significant throughput.

The incumbent technology for desalination is reverse osmosis (RO) due to its technological maturity and ability to treat a wide range of feedwaters. However, suspended solids may cause RO (and other dissolved solids removal technologies) to become clogged and lose performance. A common strategy uses dead-end filters upstream of RO systems, but membrane-based filters, including the dead-end prefilters, commonly upstream of reverse osmosis membranes, easily clog and require regular maintenance.

Unlike membrane filters, mesofluidic inline separators provide suspended solids removal with much lower pressure drops than conventional filtration systems, permitting substantially higher flow rates [2, 3]. Mesofluidic inline separators have remarkably smaller footprints than competing filtration technologies, are easily transportable between jobsites, are tunable for particle sizes of interest, are fully passive, and have no moving parts so that solids removal can be accomplished at much lower cost [4, 5]. Instead of bulky rate limiting filters to remove suspended solids, this technology fits simply within standard schedule pipes to operate at industrial flow rates and

meet safety standards and regulations [5]. The separator does not require multiple operators but can be readily operated using a single pump (perhaps even gravity flow with sufficient head/gravitational drop). Because these systems are now produced by rapid advanced manufacturing techniques, deployment can be very fast.

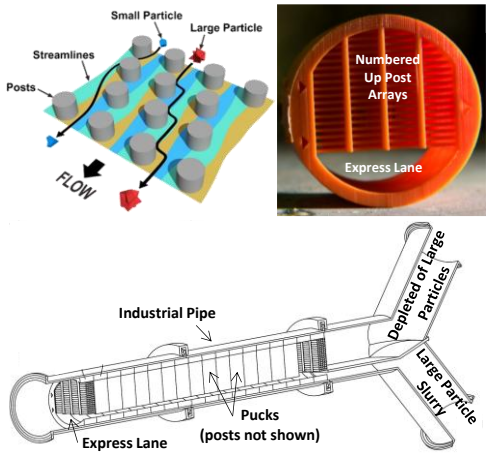

FIGURE 1. (UPPER LEFT) SCHEMATIC OF PHYSICS OF MESOFLUIDIC INLINE SEPARATOR SHOWING THAT SMALL PARTICLES SLALOM THROUGH THE POSTS WHILE LARGE PARTICLES CONSECUTIVELY BUMP TO ONE SIDE DUE TO POST STAGGERING [3]. (UPPER RIGHT) 3D PRINTED PUCK WITH POSTS THAT DRIVE LARGE PARTICLES INTO THE OPEN "SMILEY" VOLUME TERMED THE EXPRESS LANE NEAR THE BOTTOM [5]. (LOWER MIDDLE) ENGINEERING DRAWING OF PUCKS WITHIN A PIPE HOUSING THAT DIVIDES THE FLOW INTO A LARGE PARTICLE ENRICHED STREAM FROM THE EXPRESS LANE AND A PARTICLE DEPLETED STREAM [4].

Mesofluidic inline separators are passive inserts that fit within existing piping systems. These separators leverage techniques learned over decades of microfluidic advances but have been scaled up to operate at industrially relevant conditions [6]. Mesofluidic inline separators draw inspiration from a microfluidic system that originally separated the constituents of blood (e.g., red from white blood cells from platelets) and are now used to diagnose some cancers. These separators have been scaled up to accommodate broad particle size distributions, to modularly fit within three-inch pipes (see Fig. 1), and to operate at flowrates >100 gpm (as opposed to ~10 mL/h) [5]. Like microfluidics, numbering up is a key to rapid deployment [6]. Once the technology has been scaled up in a laboratory environment, modular separating elements are assembled into pucks, multiple modular pucks are assembled into a separation stage, and multiple separation stages may be assembled into a separations cascade where multiple separation targets are required to satisfy product specifications (see Fig. 1). Multiple cascades may number up to achieve a target throughput [7]. Therefore, demonstrating separation precision at the laboratory scale is substantially similar to the separation precision achieved at deployed scale. In this manner, the cost and time to cross the "valley of death" from early prototypes to commercial product is substantially reduced.

Mesofluidic separators are not membranes. Physically, mesofluidic inline separators partition particles by their size. The key to the technology[1] is the interaction among fluid flow fields, particles and posts. Small particles follow the streamlines set by staggered posts in contrast to larger particles that cannot and so must consecutively flow to one side of the posts (Fig. 1 upper left). The post array is housed in a pipe with an open space along one side called an express lane (bottom open region in Fig. 1 upper right). Under flow, the post array forces large particles into this express lane. At the end of a post array (Fig. 1 lower middle), the flow is simply partitioned with the express lane flow going one direction and the remaining flow depleted of large particles going another (i.e., to RO units).

TABLE 1. SELECT PROOF-OF-PRINCIPLE PROTOTYPES.

Scale	Form factor – material	Particle size cutoff*	Slurry	Flow rate
Bench scale	Block – polymer	700 μm	Glass beads in water	1-2 gpm
Lab scale	Block – polymer	700 μm	Glass beads in water	Up to ~4 gpm
Engineering	Cylinder – metal	40 μm	Caustic simulants	~0.5 L/min
"Half" scale	Puck – polymer	520 μm	Abrasive simulant	90-100 gpm

*Based on formula of [8] were flow to have been laminar. Bench and lab scale devices had an equilateral rhombus arrangement of pins with a pin diameter of 1.2 mm, a pin gap of 1.8 mm and an offset of 0.3 mm. The engineering scale device had an equilateral rhombus arrangement of pins with a pin diameter of 0.5 mm, a pin gap of 0.3 mm and an offset of 0.0101 mm. The "half" scale device had a rhombus arrangement of pins with a pin diameter of 1.2 mm, a flow wise pin gap of 1.815 mm, a transverse pin gap of 1.34 mm, and an offset of 0.3 mm.

We have designed, constructed and tested several prototypes of increasing complexity as shown in Table 1, each using rapid advanced manufacturing techniques. The flowrates and size separation targets were motivated by a nuclear waste processing application but suggest the capability of these separators for a broad range of applications [4]. The bench scale prototype was constructed with post between parallel plates (i.e., a block form factor; see Fig. 1 with four vertical parallel plate separators stacked together above the express lane) and demonstrated particle separation at turbulent flowrates using a gravity drained flow system with transient concentration pulses [3]. The lab scale prototype was a substantially longer version of the bench scale (>3 ft; too large to fit on benchtop) with 13 channel output

[1] U.S. Application No. 16/395,097 pending.

to evaluate particle distributions across the separator outlet. The engineering scale prototype was constructed of ~5300 posts in a super nickel alloy similar to stainless steel with a circular external form factor [2]. This prototype showed that mesofluidic inline separators are competitive versus metal dead-end filters in terms of particle size separated but at ~10 times more flow at the same pressure drop, suggesting operation orders of magnitude longer without clogging. The half scale prototype (Fig. 1) had a 3 inch external diameter with twenty pucks stacked together within a stainless steel tube to form a single separator module [5]. This prototype showed that polymer inserts performed well despite an abrasive simulant in an industrial high bay environment. Together, these studies validate the performance of mesofluidic inline separators relative to performance predictions and show that cutoff sizes tested (~40-600 µm) span much of the range of suspended solids to be removed in produced water treatment.

In this paper, we show that mesofluidic inline separators can be coupled with a commercial dissolved solids removal technology (RO) and quantify the increase in the dead-end filter lifetime before clogging.

MATERIALS AND METHODS

Unique produced water samples were obtained from two wells in the Permian Basin in West Texas (see Fig. 2). The particle size distributions from these two sites had a d_{50} of 16-31 microns for 33-28 #2H, and a d_{50} of 7-11 microns for 33-28 B#3H (see Fig. 3). The d_{90} is 30-81 microns for 33-28 #2H (overlapping at least partially the size range of the MoSci 63-90 micron particles used in these experiments to represent larger minimally setting particles found in produced water). These particle sizes are consistent with the slow settling that was observed. The particle size distribution emerging from wells varies over time, and these larger particles are likely typical of proppant, cuttings, and larger particulate remaining from the initial fracturing process.

The fully assembled system (see Fig. 4) can achieve pressures of 300 psi max. This safety limit restricts the salt concentration through the RO system to approximate 5000-7000 ppm, which lies within the TDS range of US produced waters (~1100-244000 ppm) [1].

The mesofluidic device used in these tests (see Fig. 5) was custom designed with dimensions as given in Table 2. During operation, a pump (see Table 3) was used to drive flow through the system at flows given in Table 4. Instant Ocean® Sea Salt or produced water was first driven through the mesofluidic separator as shown in Fig. 4. Flow that had proceeded through the pin array within the mesofluidic separator proceeded toward the dead-end filter (Hydronix 5 micron, SDC-25-1005). The remaining fluid from the mesofluidic separator that is enriched in particles was collected. Flow emerging from the dead-end filter was also collected for further analysis and was in some cases fed to the reverse osmosis module separately (Pro+Aqua, PRO-RO-1 with high salt membrane from Fresh Water Systems Filmtec SW30-4021 Sea Water 800 GPD RO Membrane Element). After steady-state flow was achieved, particles were added incrementally. Some tests proceed only through prefilter (as a control) and some through both the mesofluidic separator and the prefilter.

FIGURE 2. IMAGES OF THE PRODUCED WATER SAMPLES FROM APEX IN VIALS. THE TWO ON THE RIGHT ARE 33-28 #2H AND THE THREE ON THE LEFT ARE 33-28 B#3H. THE VIAL ON THE LEFT WAS PULLED TWO WEEKS EARLIER THAN THE NEIGHBORING VIALS. THE BOTTOM IMAGE WAS COLLECTED APPROXIMATELY TWO HOURS AFTER PULLING FROM THE CARBOY, SUGGESTING THAT OXIDATION PROCEEDS OVER TIME.

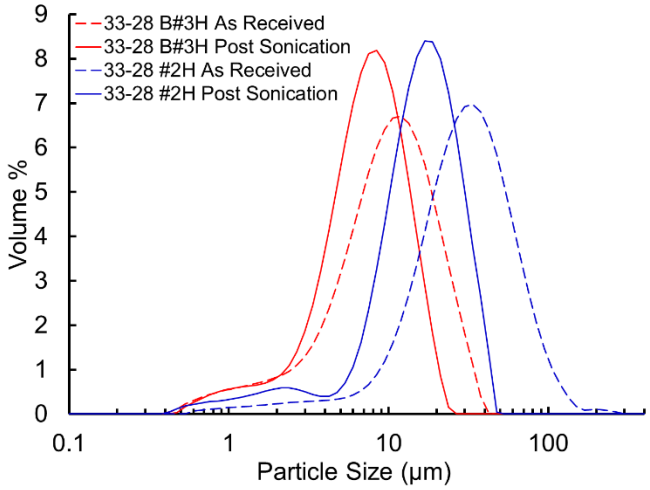

FIGURE 3. PARTICLE SIZE DISTRIBUTIONS.

FIGURE 4. IMAGE OF THE COMBINED SETUP INCLUDING A MESOFLUIDIC SEPARATOR, A PREFILTER, AND A REVERSE OSMOSIS MEMBRANE. THE MESOFLUIDIC SEPARATOR IS ON THE RIGHT IN WHITE. THE REVERSE OSMOSIS UNIT INCLUDING WHITE PREFILTER IS IN THE BLACK CART ON THE LEFT.

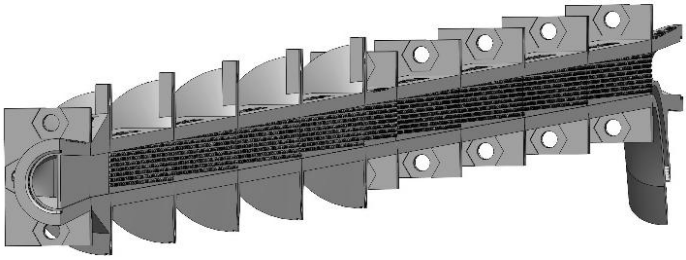

FIGURE 5. CROSS SECTION OF A MESOFLUIDIC INLINE SEPARATOR (TERMED 45-175 AFTER THE NOMINAL FUNCTIONAL RANGE IN MICRONS) WITH INLET ON LEFT AND BOTH OUTLETS ON RIGHT. LONGITUDINAL AXIS REDUCED TO FIT COLUMN WIDTH.

TABLE 2. MESOFLUIDIC INLINE SEPARATOR DIMENSIONS.

Nominal functional range	45-175 microns
Pin diameter	1 mm
Center-to-center	1.53 mm
Offset	8.2 microns
Pins in first row	7
Width available to flow	20 mm
Height	12.7 mm
Length (w/o end pieces)	2.36 m
Length (with end pieces)	2.71 m
Conical entrance angle	5.0° (w.r.t. axis)

TABLE 3. INSTRUMENTATION.

Instrument	Model
Pump	Dayton stainless steel centrifugal pump Model 5WXT1A Pump PPT05014GGG
Pressure	Digital pressure gauge (SSI Technologies, Inc. MediaGauge™ MG-50-A-9V-R) pressure transducer and an analog pressure gauge (GRIFFCO)
Flow	Magnetic-inductive flow meter (Ifm electronic magnetic-inductive flow meter SM7001)
Tank	15-gallon conical bottom
Overhead stirrer	RW16 basic IKA WERKE

TABLE 4. PERFORMANCE.

Added Mass	RO Pressure (psig)	Feed Flowrate (gpm)	Product TDS (ppm)	Product Flow Split
~0-2 kg	290-299	0.52-0.53	82-357	41-50%
Based on 4 L of produced water starting from a clean membrane based on DI water; produced water used was 33-28#2H.				

RESULTS AND DISCUSSION

The purpose of this paper is to explore how mesofluidic inline separators can be coupled or cooperatively used with a commercial dissolved solids removal technology (RO) and quantify the increase in the dead-end filter lifetime before system clogging.

Using the assembled system (see Fig. 4), we compared the performance of a prefilter with and without the mesofluidic separator installed upstream (see Fig. 4). While in some instances it may be possible to replace the prefilter with the mesofluidic separator, most reverse osmosis systems include a prefilter to ensure that a negligible quantity of particles interact with the reverse osmosis cartridge. The quantity of particles that prefilters can sustain is meaningful. For the cartridge we used approximately a kilogram of particles in Instant Ocean® Sea Salt (diluted to 5300 ppm to meet the pressure limit above) that could be loaded before the cartridge lost flow. Because we used a centrifugal pump, the flowrate may be a more sensitive indicator of cartridge performance than pressure drop. Figure 6 compares

the flowrate sustained versus the cumulative mass of particles added to the feed. The figure shows that whereas approximately ~0.7 kg of particles can be fed to the system before the dead-end filter began to clog in the absence of a mesofluidic separator (complete clogging ~1 kg); with an in-line mesofluidic separator >7 kg could be added to the system. This represents an order of magnitude factor increase in solids fed. The improved performance is not free; the pressure drop does increase from ~6 psi to ~14 psi with the addition of the mesofluidic separator.

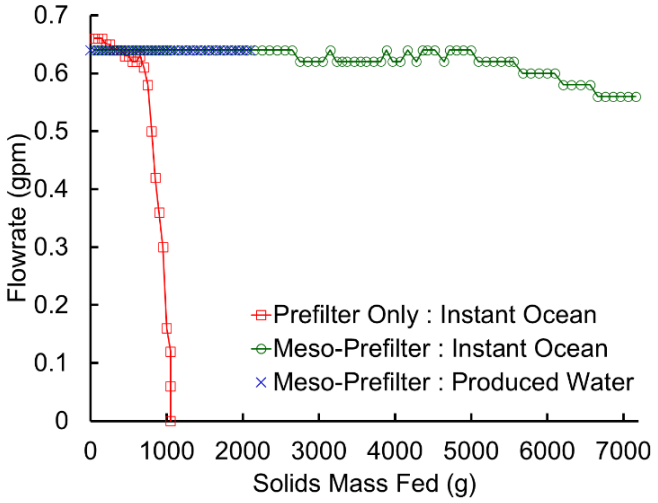

FIGURE 6. FLOWRATE AS A FUNCTION OF CUMULATIVE MASS ADDED TO THE FEED WITH AND WITHOUT THE MESOFLUIDIC SEPARATOR (NO RO).

The ultimate target of this effort is the combination of a mesofluidic separator with prefilter and a reverse osmosis membrane. Operation proceeded using unique produced water samples from the Permian Basin in West Texas diluted (to ~5300 ppm down from ~13400 ppm) to prevent the pressure drop across the membrane from exceeding 300 psi. Particles (Mo-Sci LLC 63-90 soda lime glass spheres with a size of 63-90 microns) were added to the feed tank in twice the amount necessary to ensure that in the absence of the mesofluidic separator the prefilter would have clogged, and the flowrate for the reverse osmosis membrane would have been negligibly small (see Fig. 3). The experiments showed that the performance with Instant Ocean is not distinguished from that of produced water. The water produced through the reverse osmosis membrane is not distinguishable at the beginning, middle or end of the run with produced water (see Table 4). This result indicates that mesofluidic separators can be useful in preserving the functionality of reverse osmosis systems process produced water (see Fig. 7).

Figure 8 compiles images of characteristic fluids entering and exiting the combined system. As anticipated the particle rich stream exiting from the mesofluidic separator is enriched in particles that appear white as they jet out of the separator into the beaker. Also of note is that there are three ways that flows can exit this system. Here the focus has been on removing undesirable species from the produced water. Table 4 shows that the remaining total dissolved solids is within the potable water range, though the chemical composition of those solids remains to be determined to fully ascertain whether this water would classify as potable water.

FIGURE 7. VIALS SHOWING THE (LEFT) RAW PRODUCED WATER, (MIDDLE) WATER FROM THE MESOFLUIDIC SYSTEM AND PREFILTER, AND (RIGHT) TREATED WATER FROM RO MEMBRANE.

Figure 8 also highlights that there is more than one location where species of interest could exit. For example, critical minerals could exit through either the reverse osmosis stream or alternatively be enriched in the materials trapped by the prefilter or among the particulate enriched in the mesofluidic separator.

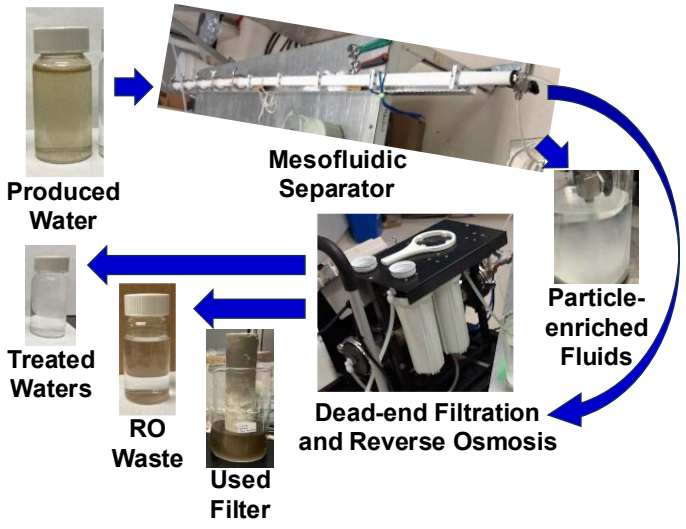

FIGURE 8. REPRESENTATION OF THE MESOFLUIDIC-REVERSE OSMOSIS SYSTEM WITH IMAGES OF THE FLUIDS AS THEY ENTER AND EXIT THE SYSTEM. THE PARTICLE RICH STREAM EXITING THE MESOFLUIDIC SEPARATOR HIGHLIGHTS A PARTICLE STREAM IN INSTANT OCEAN JETTING INTO A BEAKER. THE OTHER IMAGES ARE FOR PRODUCED WATER.

CONCLUSION

In summary, we have demonstrated removal of suspended solids from produced water using a mesofluidic inline separator. This testing is a critical step toward obtaining industry acceptance for this revolutionary technology that promises to be a key element in water treatment systems that turn produced water from a waste into a benefit (e.g., for surface discharge, reusable water, agricultural water, industrial use water, potable water, etc.).

ACKNOWLEDGEMENTS

We express appreciation to the United States Department of Energy (DOE) Fossil Energy and Carbon Management (FECM) Technology Commercialization Fund TCF-21-24900 for partial funding of this work. A portion of the research described in this report was conducted under the Laboratory Directed Research and Development (LDRD) Program as a strategic investment at the Pacific Northwest National Laboratory (PNNL), a multiprogram national laboratory operated by Battelle Memorial Institute for the U.S. Department of Energy (DOE) under Contract No. DE-AC05-76RL01830.

REFERENCES

[1] Scanlon, B., R. Reedy, P. Xu, M. Engle, J. Nicot, D. Yoxtheimer, Y. Qian, S. Ikonnikova. 2020. Can we beneficially reuse produced water from oil and gas extraction in the U.S.? Science of The Total Environment, 717, https://doi.org/10.1016/j.scitotenv.2020.137085

[2] Burns C.A., T.G. Veldman, J. Serkowski, R.C. Daniel, X.-Y. Yu, M.J. Minette, L.F. Pease. 2021. Mesofluidic Separation versus Dead-end Filtration. Separation and Purification Technology, 254, 117256. https://doi.org/10.1016/j.seppur.2020.117256.

[3] Pease L.F., J.E. Serkowski, T.G. Veldman, J. Williams, X.-Y. Yu, M.J. Minette, J.A. Bamberger, C.A. Burns. 2021. Can Bump Arrays Separate Particles from Turbulent Flows? In Proceedings of the ASME 2021 Fluids Engineering Division Summer Meeting (FEDSM 2021), August 10-12, 2021, Virtual, Online, 3, FEDSM2021-67696, V003T08A024. New York, New York: ASME. https://doi:10.1115/FEDSM2021-67696.

[4] Pease, L.F., T.G. Veldman, J. Serkowski, N.R. Phillips, R.C. Daniel, M.J. Minette, X.Y. Yu, M.S. Fountain, C.A. Burns. 2020. Efficient Mesofluidic Separation of Large Particles in Nuclear Slurries, Waste Management Symposium 2020 Proceedings, Paper 20408.

[5] Pease, L.F., N.R. Philips, J. Serkowski, T.G. Veldman, M.J. Minette, C.A. Burns. 2022. Industrial Scale Mesofluidic Particle Separation, Chemical Engineering Processing – Process Intensification 173, 108795. https://doi.org/10.1016/j.cep.2022.108795

[6] Huang, L.R., E.C. Cox, R.H. Austin, J.C. Sturm. 2004. Continuous particle separation through deterministic lateral displacement. Science, 304, 987–990. https://doi.org/10.1126/science.1094567.

[7] Pease, L.F., J.A. Bamberger, C.A. Burns, and M.J Minette. 2022. Concentrating Slurries Mesofluidically for Nuclear Waste Processing. Proceedings of the ASME 2022 Fluids Engineering Division Summer Meeting, FEDSM2022-87708 American Society of Mechanical Engineers, New York, NY. https://doi.org/10.1115/FEDSM2022-87708.

[8] Inglis, D.W., J.A. Davis, R.H. Austin, J.C. Sturm. 2006. Critical Particle Size for Fractionation by Deterministic Lateral Displacement Lab Chip, 6, 655–658. https://doi.org/10.1039/B515371A

Pacific Northwest National Laboratory

902 Battelle Boulevard
P.O. Box 999
Richland, WA 99354
1-888-375-PNNL (7665)

www.pnnl.gov